Available online at www.sciencedirect.com
ScienceDirect
Advances in Space Research 60 (2017) 1443–1452
ADVANCES IN SPACE RESEARCH
(a COSPAR publication)
www.elsevier.com/locate/asr

Compaction of montmorillonite in ultra-dry state

Brian J. Chow [a], Tzehan Chen [b], Ying Zhong [b], Meng Wang [a], Yu Qiao [a,b,*]

[a] *Department of Structural Engineering, University of California, San Diego, La Jolla, CA 92093-0085, USA*
[b] *Program of Materials Science and Engineering, University of California, San Diego, La Jolla, CA 92093, USA*

Received 4 April 2017; received in revised form 30 June 2017; accepted 2 July 2017

Abstract

The current study discovers that uniaxial compression under ambient condition can directly cause strong bonding in ultra-dry montmorillonite, which is attributed to the secondary molecular interaction other than hydrogen bonding. The strength of so-processed material is sensitive to the lateral confinement condition of loading. Similar compaction pressure produces equally strong solids between quasi-static and impact loading modes. Gas permeability of the compacted solids is comparable to those of dense rocks. These findings shed light on the study of Martian regolith and in-situ resource utilization.

Keywords: Montmorillonite; Compaction; Martian regolith; In-situ resource utilization

1. Introduction

Montmorillonite is one of the oldest engineering materials known to humankind. It consists of stacked silica-alumina lamellae (Odom, 1984). Isomorphous substitution imparts an overall negative surface charge, balanced by cations associated with an affinity for water (Sposito, 1984). Traditional processing of clay requires substantial interlayer water, often provided with 5–15 wt% additional water (Smith and Austin, 1989; Das, 2010), and sometimes energy-consuming calcinations at high temperatures up to ~1000 °C (Callister, 2003).

Increasing attention is being paid to habitability on Mars (Bell and Hines, 2005). Space transportation constraints and environmental challenges currently limit the size and complexity of habitats (Drake et al., 2010). It remains a primary target that larger Martian bases or outposts can be constructed, maintained, and expanded by using only locally harvestable resources, such as Martian regolith.

A substantial amount of smectite clay minerals have been detected on Mars (Poulet et al., 2005), including montmorillonite (Clark III et al., 2007; Ehlmann et al., 2011). They are dry, however, and cannot be processed through conventional methods (Boynton et al., 2008; Ehlmann and Edwards, 2014). A recent research discovered that primordial Martian soils may be directly compacted into strong solids, with the inter-particle bonding formed through nanophase ferric oxide (npOx) (Chow et al., 2017). If structural parts can also be produced by using secondary Martian soils, e.g. montmorillonite, the choice of materials on the Mars can be broadened.

Little experimentation has been performed on compaction of very dry montmorillonite. One envisions that clay mineral layers may be coherently bonded by secondary molecular interactions other than hydrogen bonding, if forced together closely enough (Shotton and Hersey, 1970; Karehill and Nyström, 1990). Under such a condition, interlayer water may decrease the strength of com-

---

* Corresponding author at: Department of Structural Engineering, University of California, San Diego, La Jolla, CA 92093-0085, USA.
E-mail address: yqiao@ucsd.edu (Y. Qiao).

http://dx.doi.org/10.1016/j.asr.2017.07.001
0273-1177/

pacted clay, since it increases interlayer spacing. This hypothesis is the focus of the current investigation.

2. Experimental procedure

2.1. Materials preparation

About 500 mL of montmorillonite (Sigma-Aldrich K10 69866-1kg) was placed on top of an 8-inch-diameter sieve stack, and separated with a 350 W mechanical sieve (Tyler Rotap RX-29) for 35 min. The sieve stack contained, from the top to the bottom, 5 sieve trays with the mesh sizes of 90 μm, 53 μm, 45 μm, 25 μm, and 20 μm, respectively. The particle size followed a Weibull distribution, with 90 wt% smaller than 90 μm and 50 wt% lying between 25 μm and 45 μm. About 15 mg of sieved montmorillonite powders were added to a thermogravimetric analysis (TGA) machine (Perkin Elmer Pyris 1 TGA). The rate of temperature increase was 5 °C/min; the maximum temperature was 1000 °C; the hold time at maximum temperature was 20 min. The sample was furnace-cooled to ambient temperature after the test. Nitrogen was used to purge the TGA furnace.

Fig. 1 shows typical TGA results. The steep mass loss in the 50–100 °C and 400–500 °C regions of as-received material corresponded to the well-known emissions of free water and structural hydroxyl water, respectively (Grim, 1968; Odom, 1984; Joshi et al., 1994). To reach the Martian surface soil water content around 2–5 wt% (Boynton et al., 2008), the montmorillonite was dried in a vacuum oven (Carbolite CTF 12/75/700) at 600 °C for 10 h and then air cooled; the temperature increase rate was 5 °C/min. Such a criterion represents a conservative measure because hydroxyl water is stable in secondary Martian soils (Ehlmann and Edwards, 2014).

2.2. Quasi-static compaction with various boundary conditions

The dried montmorillonite was compacted quasi-statically. Three different conditions of lateral boundary of compressive loading were tested. The first was rigid lateral boundary (Fig. 2a): Dried montmorillonite was added inside of a 19.1-mm or 12.7-mm circular steel die and compressed to the prescribed peak pressure, using an Instron 5582 machine. The loading rate was 1 mm/min. The resulting disc was extracted by pushing the sample out from one side using a 1-ton arbor press while applying a reverse manual pressure on the other piston for stability. The compression pressure was calculated as the compression force divided by the piston cross-sectional area.

The second was free lateral boundary (Fig. 2b): Dried montmorillonite was added inside of either an 8.7-mm or 19.1-mm round steel die and compressed to 150 MPa using an arbor press to form precursor pieces. The thickness of a precursor piece was around 2–3 mm. The precursor was removed and re-inserted concentrically in between piston surfaces matching either a 19.1-mm or 50.4-mm round die, respectively, such that it was compressed between flats of the piston without contact with the inner wall of the die. The die was compressed to the prescribed peak pressure in the displacement-controlled mode, by an Instron 5582 machine or a SATEC machine (M600XWHVL) for the 19.1-mm and 50.4-mm dies, respectively. The loading rate was 6 mm/min. The nominal compression pressure was calculated as the force divided by the initial cross-sectional area of precursor. Flash material was removed from the sides, and the compacted sample was extracted manually.

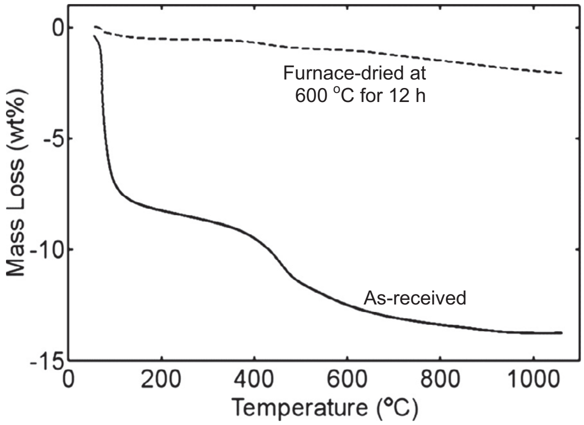

Fig. 1. Typical TGA curves of montmorillonite samples.

The third was flexible tube boundary (Fig. 2c): Steel pistons of diameter 19.1 mm were fitted with polyvinyl chloride (PVC) tubing (Finger Lakes Extrusion Clearflex 70-1 8170-2590) with inner diameter 19.1 mm, wall thickness 3.2 mm, and height 30 mm. About 5 g of montmorillonite was packed inside of the PVC tube. No adhesive or lubricant was used, as there was sufficient interference friction around the steel pistons to seal the powders. The assembly was inserted concentrically in between the loading plates of the Instron 5582 machine and compressed to the prescribed peak pressure at a loading rate of 6 mm/min. The loading condition was somewhat similar to a geotechnical triaxial test but without hydrostatic control and with a stouter sample (Das, 2010). The nominal compression pressure was calculated as the force divided by the piston cross-sectional area. The exterior of the tube was exposed to ambient. Flash material was removed throughout the tube, and the compacted sample was extracted manually.

In these compression tests, the peak pressures were chosen so that further increasing them would not lead to significant improvement in sample strength.

2.3. Impact compaction with various boundary conditions

Compaction was also performed through drop-tower impact. Free lateral boundary was achieved by using the setup shown in Fig. 3(a): Montmorillonite precursors were produced in an arbor press at 150 MPa inside of a closed circular steel die of diameter 8.7 mm. The height of the pre-

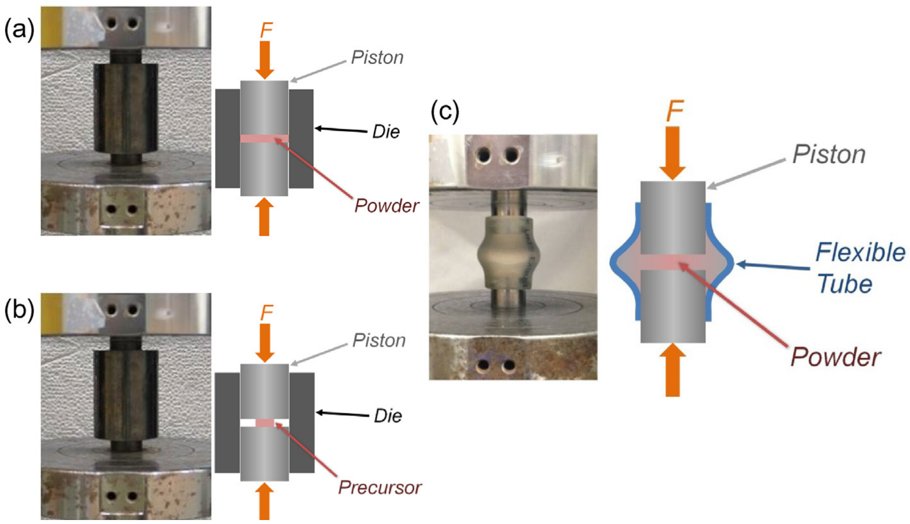

Fig. 2. Photos and schematics of quasi-static forming methods. (a) Rigid lateral boundary. (b) Free lateral boundary. (c) Flexible tube boundary.

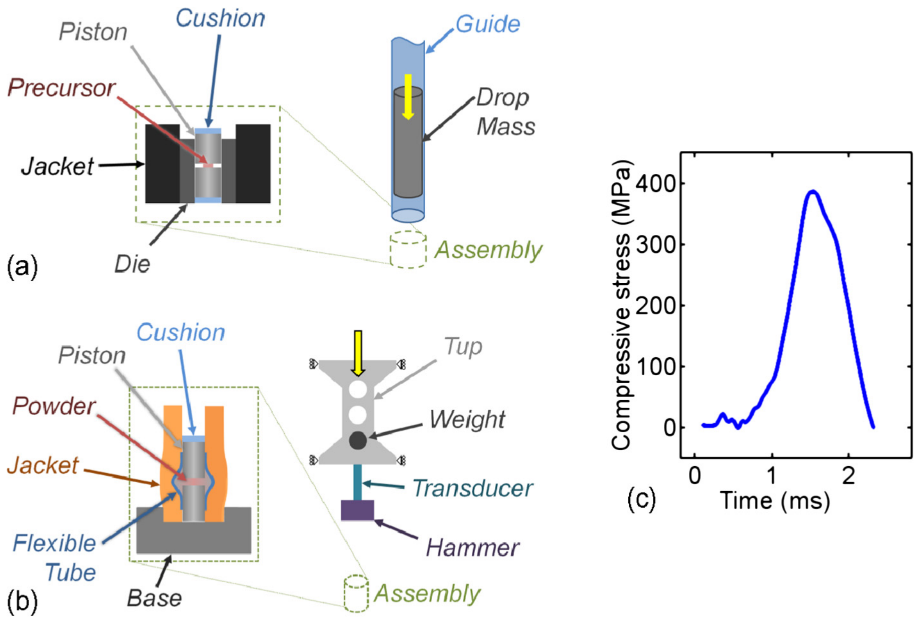

Fig. 3. Impact forming methods. (a) Setup adapted to free lateral boundary. (b) Setup adapted to flexible tube boundary. (c) Typical stress-time history of a 120-J impact.

cursor was around 2–3 mm; the diameter was ~5 mm. The precursor disc was inserted into a larger 19.1-mm-diameter steel die assembly, such that it was compacted between the flats of the die pistons without contacting the inner wall of the die. The die was inserted inside of an interfering polyurethane jacket (Pleiger Plastics MCTB9595145B) using an arbor press. The jacket and the die were secured to a fixture using U-clamps. The jacket exceeded the height of the die by 1–2 mm when the bottom faces were flush. To protect the assembly, cushions were made by compressing 1 gram of corrugated aluminum foil to 2-mm-thick discs inside a 19.1-mm diameter die at a pressure of 20 MPa. One cushion was positioned at the bottom of the assembly, and the other was positioned on top over the piston. A cylindrical drop mass of diameter 63.5 mm weighing 7.6 kg was dropped from a certain distance. A guide tube maintained the drop mass orientation, and was secured over the top of the jacket by U-clamps to a fixture holding the jacket. No leakage of the powders during the impact compression was observed. The U-clamp was removed, and the sample was released. Flash material was removed and the compacted montmorillonite was extracted manually.

Flexible tube boundary was achieved by the setup shown in Fig. 3(b): Dried montmorillonite was packed inside a Tygon tube (Saint Gobain Tygon R-3603 AAC00037) of outer diameter 12.7 mm, wall thickness 2.4 mm, and length 40 mm, and fitted around two steel pistons of diameter 12.7 mm and height 25.4 mm at each end, with the powder column length of ~25 mm. The assembly was inserted inside of an elastomer jacket (Thomas Scientific 9544T65) of outer diameter 38.1 mm, inner diameter 19.1 mm, and height 74 mm, and lightly pressed using an arbor press to introduce interference. The bottom of the jacket was fitted to a cylindrical steel cup-shaped base of outer diameter 63.6 mm, bore diameter 38.5 mm, bore depth 10.4 mm, and height 25.4 mm. When the jacket was capped on one end with the base, the bore flat sat flush with the bottom piston. The top piston was approximately 20 mm below the top of the jacket. To protect the assembly, cushions were produced by compressing 0.5 g of corrugated aluminum foil to 2-mm-thick discs inside a 12.7-mm diameter die at the pressure of 40 MPa. One cushion was placed over the top piston. The assembly was mounted on an Instron CEAST 9350 drop tower. The total drop mass, m, ranged from 2.7 to 5.7 kg. The drop distance, d, ranged from 1.8 m to 3.4 m, corresponding to velocities from 5.9 to 8.1 m/sec. No leakage of the powders during impacts was observed. Flash material was removed from within the tube, and the compacted montmorillonite was extracted manually.

2.4. Flexural strength measurement

Compacted montmorillonite discs were cut and ground into beam samples using a MTI SYJ-40-JD saw and 600-grit sandpapers. The edges of the beams were lightly chamfered by 1500-grit sandpapers. The depth of the beam was identical to the thickness of the disc, while both the length and width were cut from the diameter of the disc. Beam samples were placed on three-point bending fixtures, as shown in Fig. 4. The span lengths were 5.0 mm, 9.8 mm, or 15.2 mm, depending on the fixture used. A top point-load applicator was placed at the middle point. The fixture was centered with respect to the point-load applicator by using a caliper. The loading rate was set at 6 mm/min. The maximum force at the onset of final failure, F_m, was measured. The flexural strength, R, was calculated as $R = 3F_mL/2bt^2$, where L is the distance between the two supports and b and t are the width and the thickness of the sample, respectively. A minimum of 4 flexural tests were performed for each configuration. The time between the onset of furnace drying and the final flexural strength measurement was less than 12 h. At rest, the samples were kept in a sealed container in an oven at 110 °C. Fig. 5 shows typical measurement results.

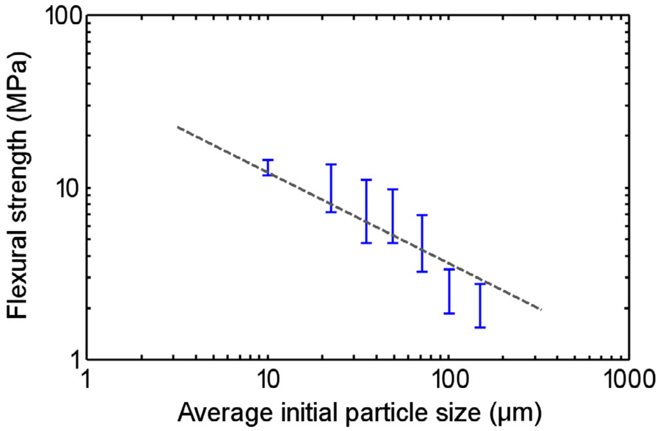

Fig. 5. Flexural strength of compacted montmorillonite samples as a function of the initial particle size. Montmorillonite was dried at 110 °C and compressed to 360 MPa, with the rigid lateral boundary. Linear regression is shown by the dashed line.

2.5. Control of water content prior to, during, and after compaction

Loose montmorillonite was dried to 90 °C, 110 °C, 190 °C, 270 °C, 350 °C, 400 °C, 500 °C, or 600 °C for 10 h. The dried powders were each quasi-statically compacted with rigid lateral boundary and the flexural strength was measured. The highest strength and the lowest strength data of each type of samples were procedurally rejected. Arithmetic means were computed from a minimum of 4 samples. Table 1 lists the average flexural strengths.

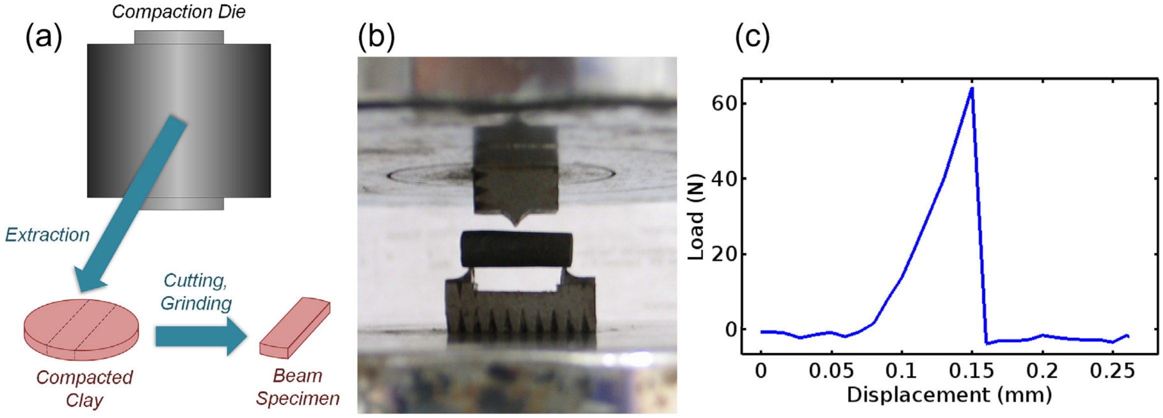

Fig. 4. Beam sample preparation and testing. (a) Schematic of the procedure of beam sample preparation. (b) Photo of the three-point bending setup. (c) A typical load-displacement curve of flexural strength measurement test.

Table 1
Average flexural strengths of montmorillonite treated to different temperatures and compacted with rigid lateral boundary.

Drying temperature [°C]	Average Flexural Strength [MPa]
90	8.93
110	7.81
190	3.66
270	4.48
350	3.45
400	3.63
500	4.13
600	2.29

Water content was also adjusted during compaction. Montmorillonite was dried at 600 °C for 12 h, and 8.7-mm-diameter precursors were made. The precursor was extracted and weighed on an Ohaus digital balance. One to two drops of water were then added to the precursor using a pipette. Rehydrated precursors were dried in a VWR 1330GM oven at 102 °C for various durations to achieve the following prescribed water contents: 2.3 wt%, 7.8 wt%, or 16.8 wt%. Water content was probed by weighing intermittently every 10 min. The total drying time ranged from 10 min to 2 h. When the prescribed water content was achieved, the precursor was compacted with free lateral boundary. The compacted montmorillonite was dried at 100 °C for 2 h and tested for flexure strength measurement. The highest and lowest data were procedurally rejected. This procedure was performed for three initial particle sizes: less than 20 μm, 25–45 μm, and 53–90 μm. Fig. 10 plots the flexural strength as a function of the added water content.

In addition, sample drying was conducted after compaction. Loose montmorillonite was dried in oven at 110 °C for 5 h, and quasi-statically compacted with rigid lateral boundary to 360 MPa. No water was added. Only the 19.1-mm die was used. The compacted sample was heated in a quartz tube furnace (Carbolite CTF 12/75/700) at 350 °C for 4 h. After heating, flexural strength was measured. The highest and lowest data were procedurally rejected, and the mean strength was calculated from 4 valid tests.

2.6. Gas permeability measurement

Compacted Montmorillonite samples were produced with rigid lateral boundary, using a 19.1-mm-diameter steel piston under quasi-static loading. The compacted samples were ground into round discs using 600-grit and 1500-grit sandpapers in the profile of a 12.7-mm-diameter control piston.

The reference piston was inserted into Tygon tubing and secured with a hose clamp. The Tygon outlet led to an upside-down 100-ml graduated cylinder filled with water in a tank, and the inlet was connected to a 138-kPa gauge nitrogen gas source. No nitrogen leakage through the control piston could be detected in 30 min.

The montmorillonite specimen was inserted into the Tygon tube assisted by the reference piston, and sealed around the edges with silicone vacuum grease (Dow Corning, Midland, MI). The hose clamp was lightly tightened around the specimen. Upon removal of the reference piston the hose clamp was fully tightened, and then connected to the graduated cylinder. The inlet was opened. The amount of time required to fill most of the graduated cylinder was recorded, and permeability was calculated as (Paulini and Nasution, 2007): $Q\left(\frac{2\mu_d t_0}{A_1}\right)\left(\frac{P_o}{P_i^2-P_o^2}\right)$, where Q is average volumetric flow rate, μ_d is dynamic viscosity, t_0 is thickness of the sample, A_1 is the cross-sectional area, P_o is the ambient pressure, and P_i is the upstream pressure. A schematic representing the setup is shown in Fig. 11. Four specimens were tested, as shown in Table 2.

3. Results and discussion

Small amounts of free water help strengthen ordinary air-dried clays upon compaction (e.g. Smith and Austin, 1989). Martian clays may be similar to dehydroxylated clays, and their behaviors are unclear. One of the objectives of the current study is to investigate whether ultra-dry clays can still strengthen with appropriate compaction techniques. We substitute geologic time of Martian clays with elevated drying temperature of our testing samples. Actual Martian clays are expected to behave somewhere in between fully moisturized terrestrial clays and the ultra-dry clay discussed below.

The results of the experiments indicate that oven-dried montmorillonite powders can be directly compacted into strong solids (Fig. 6a). Fig. 12 shows a typical stress-displacement curve during forming. The sample hardens to be more linear-elastic between 360 MPa and 800 MPa; particle motion gradually ceases, representing where the sample gains much strength.

Typical dimensions of the beam specimens are shown in Table 3. After compaction, the ratio of the disc thickness to diameter substantially depended upon the boundary condi-

Table 2
Permeability measurement results.

Sample no.	Thickness [mm]	Section Area [mm^2]	Elapsed Time [s]	Volume [ml]	Permeability [10^{-17} m^2]
1	3.61	136.9	1809	90	9.97
2	2.92	135.6	1900	80	6.89
3	2.82	134.0	4322	102	3.77
4	2.56	122.9	6023	91	2.39

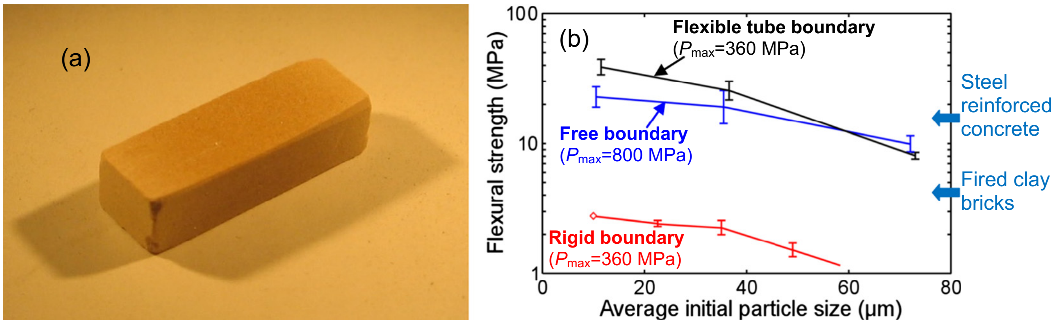

Fig. 6. Quasi-static compaction of montmorillonite. (a) Solid montmorillonite beam sample produced from quasi-static compaction with flexible tube boundary; the beam length is 1.2 cm. (b) Flexural strengths of quasi-statically compacted samples with various average initial particle sizes (D), lateral boundary conditions of compressive loading, and peak compression pressures (P_{max}).

Table 3
Typical beam specimen sizes.

Boundary condition	Length [mm]	Width [mm]	Thickness [mm]
Rigid	19	4	1.5
Free	5	2	0.5
Flexible	10	3	3

tion of compressive loading. Significant geometry differences between quasi-static and impact compaction, however, were not discerned. Between free and flexible tube boundaries, the former resulted in a more slender ratio. That is, with the partial confinement from the tubing, the flexible tube boundary helped increase the sample thickness, even when accounting for the difference in compression pressure.

Under quasi-static loading, if the montmorillonite particles are confined by rigid mold, the strength of compacted sample is quite low, lower than that of ordinary clay bricks (Plummer, 1939). Free and flexible tube boundaries lead to much higher flexural strengths, as shown in Fig. 6(b). In general, the flexural strength, R, increases with the peak compression pressure, P_{max}. The value of P_{max} is assessed as $P_{max} = F_{max}/A_0$, where F_{max} is the peak compressive force and A_0 is the initial sample cross-sectional area.

With the flexible tube boundary, similar flexural strength can be reached at a much lower peak pressure than the free lateral boundary. With flexible tube or free lateral boundary, the flexural strength is comparable with or higher than that of steel reinforced concrete (Limbrunner and Aghayere, 2010). With optimum P_{max}, the free and flexible tube boundaries do not significantly differ in strength, but the latter exhibits greater sensitivity to variations in initial average particle size. As the initial particle size, D, decreases, R tends to increase. When D is below 20 μm, flexible tube boundary results in the highest flexural strength ~45 MPa.

Clearly, particle rotation and shearing promotes bond formation, as it decreases interlamellar distance and aligns the lamellar structure. Since both rotation and shearing demand lateral motion, the confinement along the transverse direction should be quite weak to accommodate the most energetically favorable configurations. Large-scale lateral motion is unnecessary because small-particle motion tends to be local; thus, the free and the flexible tube boundaries result in somewhat similar strength. SEM microscopy shows the alignment of clay mineral layers in compacted samples (Figs. 7a and 8). Confinement provided by the flexible tube used in the current study is likely not optimal. It is possible that by further adjusting the wall thickness and material, sample size and strength may be improved.

Fig. 7(b) suggests a weak loss in long-range order after compaction. It implies a disruption on the interlamellar characteristic length scale and should be attributed to the shear separation of clay mineral layers in the dry state. Consider a lamellar stack undergoing Mode II shear loading. According to (Tada et al., 2000), the critical shear stress $\tau_{cr} = \sqrt{2E\gamma/[\pi a_p(1-\nu^2)]}$, with E being the effective Young's modulus, γ the surface energy, a_p the characteristic length, and ν the effective Poisson's ratio. Based on reference data in open literature (Davidge and Tappin, 1968; Wiederhorn, 1969; Helmy et al., 2003; Manevitch and Rutledge, 2004) and with the initial particle size being taken into consideration, the parameter values can be assessed as $E \approx 50$ GPa, $\gamma \approx 0.2$ J/m^2, $a \approx 1$ μm, and $\nu \approx 0.3$. The resulting critical compression pressure is $\sigma_{cr} \approx 2\tau_{cr} \approx 170$ MPa, without lateral constraint. With frictionless lateral constraint, $\sigma_{cr} \approx 3.5\tau_{cr} \approx 290$ MPa. Both calculated stresses lie well below the peak compression pressures during compaction, 360–800 MPa. The flexible tube and rigid lateral boundaries lead to significantly greater sample thickness than the free lateral boundary. Without lateral confinement, the particles tend to be widespread. With the flexible tube, a radial confinement that "coaxes" local hardening is promoted. If the boundary condition is rigid, while the sample thickness is relatively large, the particle rotation and shearing are suppressed and the defect density, therefore, tends to be high.

Initial particle size is an important factor. The R-D curves fit well with the well-known Orowan-Knudsen relation (Shotton and Hersey, 1970): $kD^{-\beta}$ (Fig. 5), where $k^* \approx 40$ and $\beta = 0.525$ are system parameters for stress in

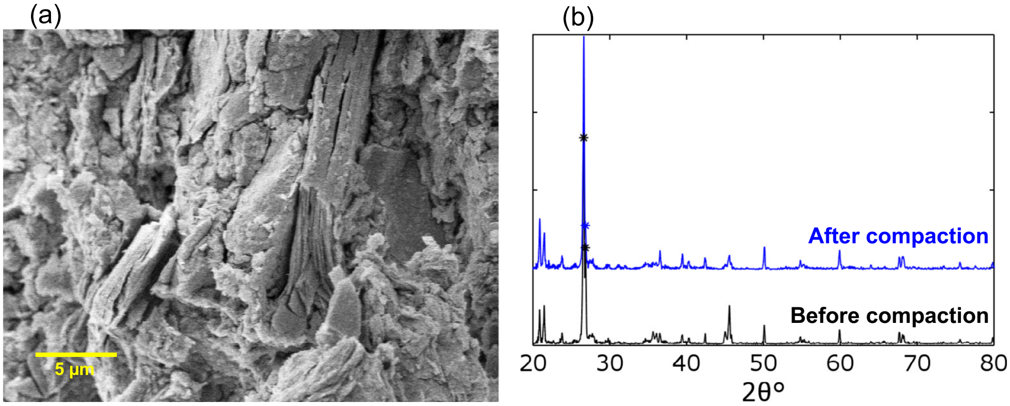

Fig. 7. (a) Typical SEM image showing particle shearing; the sample was compacted with the flexible tube boundary and initial particle size 25–45 μm; the compressive loading was 360 MPa, applied along the horizontal direction. (b) XRD analysis results before and after quasi-static compaction to 360 MPa with the same process configuration; asterisks indicate peaks.

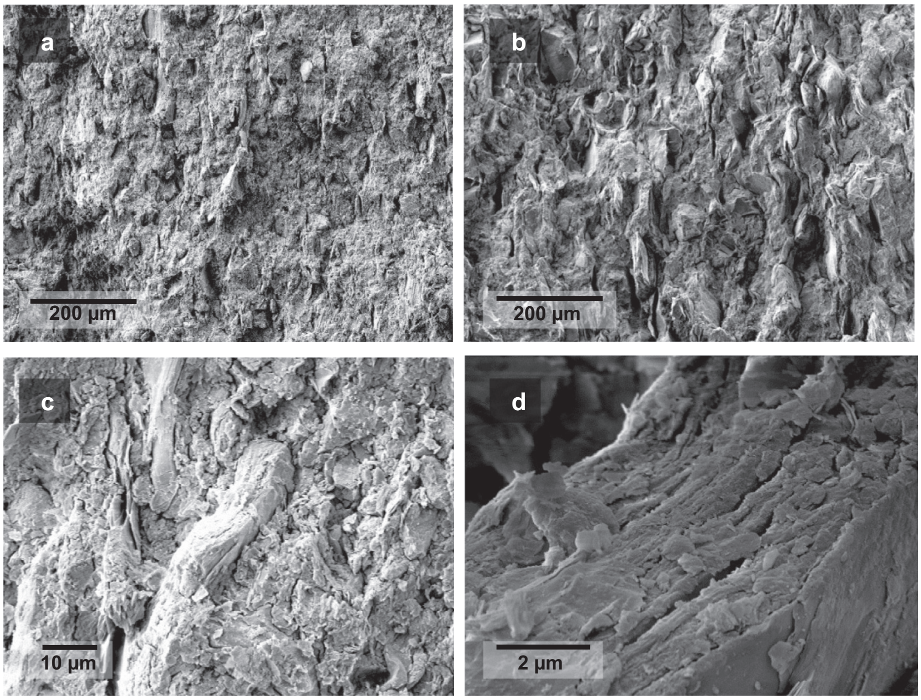

Fig. 8. SEM images of fracture surfaces of samples processed with flexible tube boundary, with the initial particle sizes of (a) 25–45 μm and (b) 53–90 μm, respectively. (c) Sheared particles and (d) a high-resolution image. Compressive loading was applied along the horizontal direction.

MPa. Smaller sizes of particles exert less resistance to particle shearing, and also increase the specific surface area, *i.e.*, the available interface area for bond formation. The slightly greater sensitivity of the flexible tube boundary relative to the free lateral boundary may be related to the inhibition of void formation during lateral spreading. Since smaller particles have more localized movement, macroscopic lateral expansion during compaction would tend to form more voids.

Under impact loading, the samples produced with rigid lateral boundary are fragile and no strength can be measured. Free or flexible tube boundary yields strong, intact specimens. As shown in Table 4, the free lateral boundary results in the greatest flexural strength, yet at a much higher impact pressure than the flexible tube boundary. The impact pressure can be assessed if $F_{\max}$ is taken as the peak force measured by the accelerometer mounted on the drop hammer. As the impact pressure is similar with the quasi-static compressive pressure, the flexural strength of impact-formed samples tends to be higher, suggesting that the bonding formation among the particles is fast. Fig. 9(a) indicates that when the initial particle size, D, is reduced, R significantly increases. In Fig. 9(b), R would not vary much when the drop mass (m) and the drop dis-

Table 4
Flexural strengths and compression pressures.

Boundary condition of compressive loading	Quasi-static compaction		Impact compaction	
	Average flexural strength [MPa]	Optimum peak compression pressure [MPa]	Average flexural strength [MPa]	Impact pressure [MPa]
Rigid	~2	360	~0	~400
Free	23	800	45	>800
Flexible	39	360	42	~400

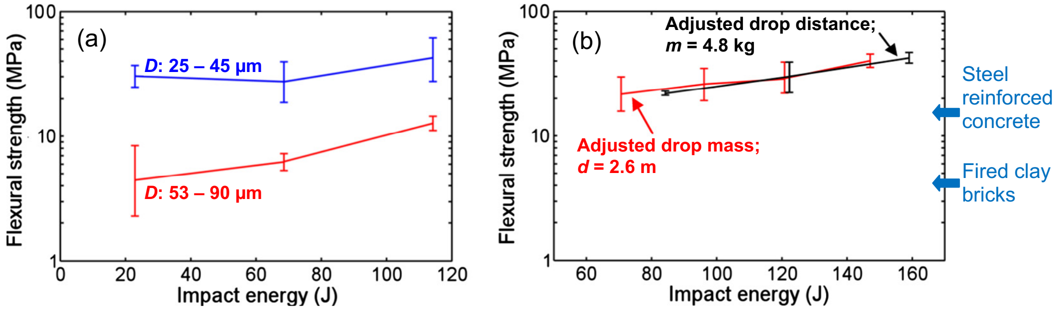

Fig. 9. Flexural strengths of impact-formed samples. (a) Dynamic compaction with free lateral boundary, with various initial particle sizes (D) and impact energy of constant drop mass. (b) Dynamic compaction with flexible tube boundary; the impact energy is controlled by adjusting either the drop distance, d, or the drop mass, m; D ranges from 25 to 45 µm.

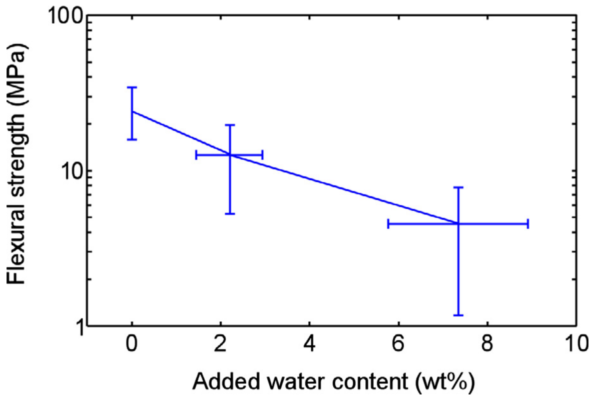

Fig. 10. Flexural strength of montmorillonite rehydrated to different water contents and compacted with free lateral boundary to 800 MPa. Initial particle size was 25–45 µm. Scatter in the target water contents is shown by horizontal error bars.

tance (d) changes broadly with similar total impact energy. In all the cases, the flexural strength rises with the impact energy.

The equivalence of the resultant flexural strengths between quasi-static and impact loading cases affirms the notion that the bonding process is relatively time-invariant. Montmorillonite lamellae are bound together upon contact between energetically favorable facets. Loading rate sensitivity was not detected because electrostatic interaction is a function of separation distance rather than time. In the current experimental configuration, impact loading has a characteristic duration of ~1 ms.

When montmorillonite is heated above normal drying temperatures prior to compaction, the flexural strength of the compact decreases (Table 1). If relatively small amounts of free water are present in the montmorillonite lamellae and allow bonds to form, heating the samples after compression should cause a reduction in strength, especially when the surface tension of hydrogen-bound water contributes to the strength. When samples were dried to elevated temperature after compaction, the mean flexural strength was 23.4 MPa, significantly higher than that of any samples without post-compression heating, suggesting that, with the processing and testing conditions under investigation, water is not a major factor that influences the strength of compacted montmorillonite.

However, it is still possible that small amounts of water can align the clay particles and hydrogen bonding is present in thinner layers if the clay mineral layers are sufficiently parallel, and lenticular voids do not form from volatile loss. This was controlled by introducing water during processing using the free lateral boundary of compaction. An overall decrease was observed as the water content increased (Fig. 10), consistent with previous findings in literature (Nichols and Grismer, 1997). The montmorillonite particles are aligned with high pressure, and the thin dimensions of the specimen minimize voids from drying stresses. Because different water contents are processed to the same forming pressure and subsequently dried to the same temperature, flexural strength should depend on the resultant hydrogen bonds in between parallel clay mineral layers. If hydrogen bonds are responsible for the strength, the flexural strength should be the same irrespective of the amount of water initially added. This was not

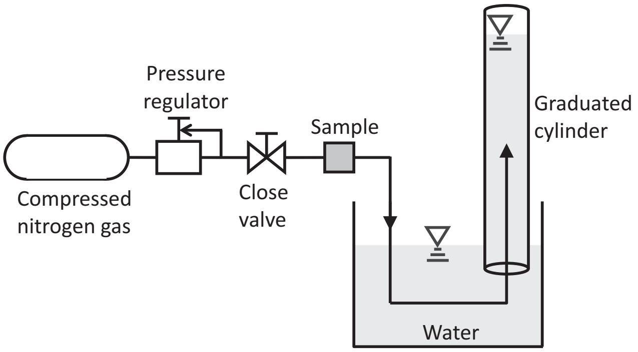

Fig. 11. Schematic illustrating the configuration of the gas permeability test setup. The main connecting line represents the flexible tubing. The pressure regulator is prescribed to 138 kPa upstream of the sample. Graduated cylinder is initially full of water to the top.

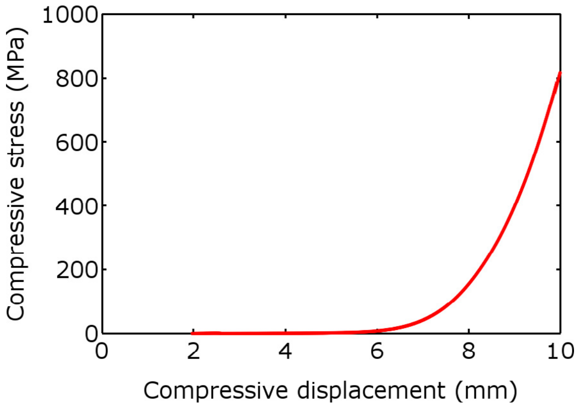

Fig. 12. A typical stress-displacement curve during forming of samples. The curve represents loading of a montmorillonite precursor dried at 600 °C, surrounded by a free lateral boundary. The peak compressive stress is 800 MPa. Substantial hardening occurs past $\sim$8 mm. Similar hardening curves describe the other lateral boundary configurations.

the trend observed, and the decrease in flexural strength with increasing water content furthers the notion that closely forced clay mineral layers experience a different type of bond under relatively dry initial conditions. Water increases the interlamellar distance, and the equilibrium distance after drying may be insufficient to develop strength.

The strength of water-bound montmorillonite should deteriorate or remain the same if water-aided hydrogen bonding contributed to the final strength (Joshi et al., 1994; Nichols and Grismer, 1997). Decreasing the flexural strength with increasing pre-compaction drying temperature introduces two possibilities: First, residual water may promote strength development; second, drying at a lower temperature may favor the predominance of hydrogen bonds. Because flexural strength increases with post-compaction drying temperature ($R \sim 23$ MPa), hydrogen bonding must not be the dominant factor of strength, supporting the second possibility. Flexural strength tends to decreases as the drying temperature exceeds the critical point associated with the removal of free water. Presence of free water would imply that a meniscus, brought about by surface tension of water together with the diffuse double layer, reaches low radius of curvature. The increase in "sharpness" would hence lead to the expectation of lowering the strength. This effect indicates that water content is not essential to the integrity of the samples made from montmorillonite dried at 600 °C before compaction. Furthermore, the decrease in strength for all added water contents prior to compaction shows that water does not promote processing at high pressures.

Overall, all three controls addressing water content present evidence against the notion of hydrogen bonding playing a substantial role in strength of compacted solids. The dominant secondary bonding between dry montmorillonite lamellae is likely caused by other Van der Waals forces, such as electrostatic interactions.

Nitrogen permeability of the compacted samples is on the order of 10^{-17} m^2 (Table 2), comparable with that of solid rocks such as granite and gneiss (Brace et al., 1968; Wang et al., 2014). It is expected from the dense structure observed in SEM. Assuming steady-state incompressible flow and neglecting the action of the diffuse double layer for gaseous transport, a $\sim$100 mm^2 area disc containing $\sim 10^{-3}$ mm^2 average particle area would have about 10^5 effective channels, through the sample thickness. As a first-order approximation, the pressurized gas motion may be modeled as a Poiseuille flow: $Q = \pi r_c^4 \cdot \Delta P / 8\mu_c L_c$, where r_c is the radius of the channel, ΔP is the pressure difference, μ_c is the dynamic viscosity, and L_c is the length. With appeal to the micrograph shown by Fig. 7(a) and the sample thickness ($\sim$3 mm), assume a radius of $\sim 10^{-7}$ m and a length of $\sim$10 cm. This leads to a permeability around 10^{-16} m^2, quite close to the experimental data. During sample failure, clay platelets may form larger voids during pull-out if the particle shape exhibits some irregularity (Fig. 8), leading to apparently larger voids. This in turn may account for the discrepancy between the assumed Poiseuille tube radius and the actual interparticle distance of an intact sample.

4. Concluding remarks

In summary, it is feasible to directly compact oven-dried montmorillonite into strong solids under ambient condition, absent from heating and extraneous water or binders. Quasi-static and impact loadings can achieve similar flexural strengths. The lateral confinement condition of compressive loading and the initial particle size are important parameters. Flexible tube or free lateral boundary leads to a much higher sample strength than rigid lateral boundary. The flexural strength of montmorillonite compacted with flexible tube boundary can be higher than that of steel-reinforced concrete. The gas permeability is comparable with those of dense rocks. Addition of water has detrimental effects, suggesting that little hydrogen bonding is invovled. Prevalence of electrostatics in the interparticle bond implies that a larger family of substances in Martian regolith may be capable of compacting into strong solids without water.

Acknowledgements

This research was supported by NASA under Grant No. NNX12AI73G. We are also grateful to Prof. Patrick J. Fox, Prof. John S. McCartney, and Dr. Donald D.N. Chow for the helpful discussions. Special thanks are due to Mr. Cheng Zhang, Mr. Juan A. Ramirez, and Mr. Cruz M. Galarza for the help with the experimental work.

References

Bell, L., Hines, G.D., 2005. Mars habitat modules: launch, scaling, and functional design considerations. Acta Astronaut. 57, 48–58.

Boynton, W.V., Taylor, G.J., Karunatillake, S., Reedy, R.C., Keller, J.M., 2008. In: Bell, J.F., III (Ed.), The Martian Surface: Composition, Mineralogy, and Physical Properties. Cambridge University Press, p. 110.

Brace, W.F., Walsh, J.B., Frangos, W.T., 1968. Electrical resistivity changes in saturated rocks during fracture and frictional sliding. J. Geophys. Res. 73 (6), 2225–2236.

Callister Jr., W.D., 2003. Materials Science and Engineering. Wiley, Hoboken, NJ.

Clark III, B.C., Arvidson, R.E., Gellert, R., Morris, R.V., Ming, D.W., Richter, L., Ruff, S.W., Michalski, J.R., Farrand, W.H., Yen, A., Herkenhoff, K.E., Li, R., Squyres, S.W., Schroder, C., Klingelhofer, G., Bell III, J.F., 2007. Evidence for montmorillonite or its compositional equivalent in Columbia Hills. Mars. J. Geophys. Res. 112, E06S01.

Chow, B.J., Chen, T., Zhong, Y., Qiao, Y., 2017. Direct formation of structural components using a martian soil simulant. Sci. Rep. 7, 1151.

Das, B.M., 2010. Principles of Geotechnical Engineering. Cengage Learning, Stamford, CT.

Davidge, R.W., Tappin, G., 1968. The effective surface energy of brittle materials. J. Mater. Sci. 3, 165–173.

Drake, B.G., Hoffman, S.J., Beaty, D.W., 2010. Human exploration of Mars, design reference architecture. In: IEEE 2010 Aerospace Conference, IEEE, Piscataway, NJ.

Ehlmann, B.L., Edwards, C.S., 2014. Mineralogy of the Martian surface. Annu. Rev. Earth Planet Sci. 42, 291–315.

Ehlmann, B.L., Mustard, J.F., Murchie, S.L., Bibring, J.P., Meunier, A., Fraeman, A.A., Langevin, Y., 2011. Subsurface water and clay mineral formation during the early history of Mars. Nature 479, 53–60.

Grim, R.E., 1968. Clay Mineralogy. McGraw-Hill, New York, NY.

Helmy, A.K., Ferreiro, E.A., de Bussetti, S.G., 2003. The surface energy of montmorillonite. J. Colloid Interface Sci. 268, 263–265.

Joshi, R.C., Achari, G., Horsfield, D., Nagaraj, T.S., 1994. Effect of heat transfer on strength of clay. J. Geotech. Eng. 120, 1080–1088.

Karehill, P.G., Nyström, C., 1990. Studies on direct compression of tablets XXI. Investigation of bonding mechanisms of some directly compressed materials by strength characterization in media with different dielectric constants (relative permittivity). Int. J. Pharma. 61, 251–260.

Limbrunner, G.F., Aghayere, A.O., 2010. Reinforced Concrete Design. Prentice Hall, Upper Saddle River, NJ.

Manevitch, O.L., Rutledge, G.C., 2004. Elastic properties of a single lamella of montmorillonite by molecular dynamics simulation. J. Phys. Chem. B 108, 1428–1435.

Nichols, J.R., Grismer, M.E., 1997. Measurement of fracture mechanic parameters in silty clay soils. Soil Sci. 162, 309–322.

Odom, I.E., 1984. Smectite clay minerals: properties and uses. Phil. Trans. R. Soc. Lond. A 311, 391–409.

Paulini, P., Nasution, F., Paulini, P., Nasution, F., 2007. Air permeability of near-surface concrete. In: Concrete Under Severe Conditions Environment & Loading. CONSEC '07 Tours, France.

Plummer, H.C., 1939. Principles of Brick Engineering. Structural Clay Products Institute, Washington, DC.

Poulet, F., Bibring, J.P., Mustard, J.F., Gendrin, A., Mangold, N., Langevin, Y., Arvidson, R.E., Gondet, B., Gomez, C., 2005. Phyllosilicates on Mars and implications for early martian climate. Nature 438, 623–627.

Shotton, E., Hersey, J.A., 1970. In: Lachman, L., Lieberman, H.A., Kanig, J.L. (Eds.), The Theory and Practice of Industrial Pharmacy. Lea & Febiger, p. 174.

Smith, E.W., Austin, G.S., 1989. Adobe, Pressed-Earth, and Rammed-Earth Industries in New Mexico. Authority of State of New Mexico, Socorro, NM.

Sposito, G., 1984. The Chemistry of Soils. Oxford University Press, Oxford, UK.

Tada, H., Paris, P.C., Irwin, G.R., 2000. The Stress Analysis of Cracks Handbook. ASME, New York, NY.

Wang, H., Xu, W., Zuo, J., 2014. Compact rock material gas permeability properties. Physica B 449, 10–18.

Wiederhorn, S.M., 1969. Fracture surface energy of glass. J. Am. Cer. Soc. 52, 99–105.